

Production of ultra-slow antiproton beams

Hiroyuki A. Torii^{*}, N. Kuroda[†], M. Shibata[†], Y. Nagata^{*}, D. Barna^{**},
M. Hori[‡], J. Eades[‡], A. Mohri[‡], K. Komaki^{*} and Y. Yamazaki^{*,†}

^{*}*Institute of Physics, University of Tokyo, 3-8-1 Komaba, Meguro-ku, Tokyo 153-8902, Japan*

[†]*Atomic Physics Lab., RIKEN, 2-1 Hirosawa, Wako-shi, Saitama 351-0198, Japan*

^{**}*KFKI, Budapest, Hungary*

[‡]*CERN, Genève 23, CH-1211, Switzerland*

Abstract.

We have recently succeeded in decelerating and confining millions of antiprotons, 50 times more efficiently than conventional methods, in an electromagnetic trap. These antiprotons were cooled by preloaded electron plasma to an energy below an electronvolt. They were then extracted out of the magnetic field of 2.5 T and transported typically at 250 eV along a beamline, designed for efficient transport at 10–1000 eV. This unique beam from our apparatus named MUSASHI opens up a new field of atomic and nuclear physics probed by ultra-slow antiprotons.

In this paper, the whole experimental setup and procedure will be overviewed: deceleration, capture, cooling and extraction of antiprotons will be discussed in detail, including technical description of diagnostic devices.

Keywords: antiproton, Antiproton Decelerator (AD), RFQD (Radio Frequency Quadrupole Decelerator), Multi-Ring electrode Trap (MRT), ultra-slow antiproton beam

PACS: 7.77.Ka, 39.10.+j, 36.10.-k, 52.27.Jt

INTRODUCTION

Since its first discovery in 1955 at Bevatron in Lawrence Berkeley National Laboratory [1], antiproton has been considered as a suitable candidate (anti-)particle for test of symmetry between matter and antimatter. With the advent of the Low-Energy Antiproton Ring (LEAR) which operated from 1982 until 1996 at CERN (Organisation Européenne pour la Recherche Nucléaire) in Geneva, low-energy antiproton physics started to flourish. CPLEAR collaboration [2] used the provided 5 MeV antiproton beam to measure precisely the parameters for CP violation between K^0 and \bar{K}^0 . Following the first successful production of antihydrogen [3], reported in the last year of LEAR operation, a plan to construct an alternative machine dedicated for studies using low-energy antiprotons came into reality as the Antiproton Decelerator (AD) [4] at CERN in the turn of the century. Two of the experimental collaborations in the AD hall, ATHENA and ATRAP, succeeded in synthesis of cold antihydrogen atoms out of trapped antiprotons and positrons [5, 6], and are pursuing their goal of spectroscopy of the anti-atom. On the other hand, our collaboration ASACUSA, as is represented by its name of origin “Atomic Spectroscopy And Collisions Using Slow Antiprotons”, is aiming at exploring a wider field of atomic physics involving low-energy antiprotons [7]. The physics program includes spectroscopy of antiprotonic helium atoms which has developed so far as to a precise determination of the antiproton mass [8], stopping-power measurements at low-energies [9], and researches on antiprotonic collision dynamics such as ionization

processes and antiprotonic atom formation [10, 11]. We are also preparing a cusp trap [12] and a Paul trap for production of antihydrogen as our near-future program.

Antiproton, as an exotic particle with infinite lifetime, is an interesting and ideal probe in atomic physics, as well as in nuclear physics. Having the same mass as the proton but with opposite charge, it acts as a “heavy electron” or as a “negative nucleus”. But in order to investigate atomic processes such as ionization and atomic capture, the antiproton as a probe particle needs to become available as a mono-energetic beam with a low energy comparable to the Rydberg energy. With the aim of decelerating and cooling the antiproton beams delivered from the AD facility at 5.3 MeV, the Trap Group of the ASACUSA collaboration prepared a sequential combination of a Radio-Frequency Quadrupole Decelerator (RFQD) and an electromagnetic trap in a strong magnetic field produced by a superconducting solenoid. The antiprotons were to be confined and cooled in the trap, before being extracted along a beamline specially designed to transport an ultra-low energy beam at 10–1000 eV.

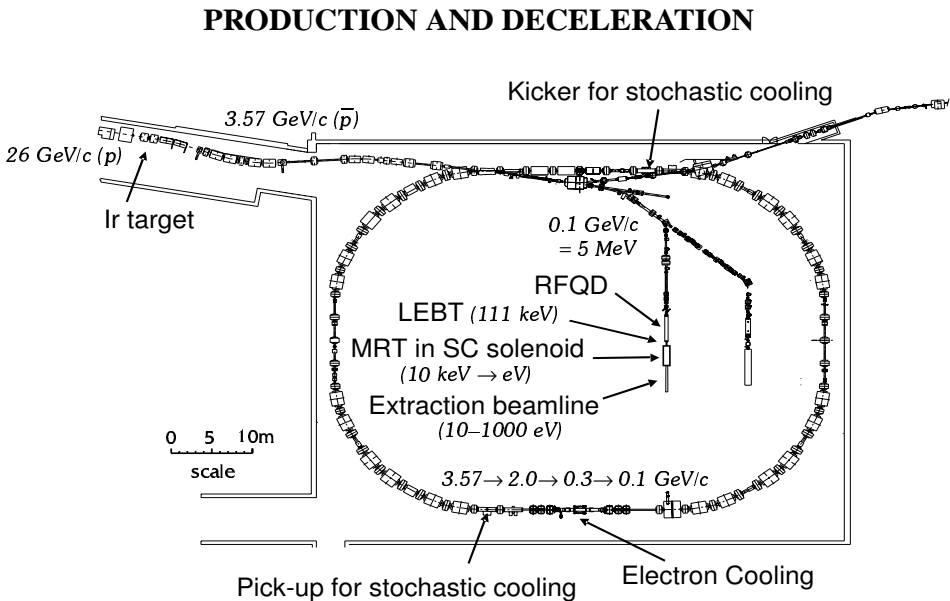


FIGURE 1. Layout of the Antiproton Decelerator (AD) at CERN.

Antiprotons (\bar{p}) are produced by protons colliding onto a fixed target above the threshold of 5.6 GeV kinetic energy in the laboratory frame. Research on antiproton is pursued also at Fermilab in the U.S., but if one wants a well-cooled low-energy beam, the Antiproton Decelerator (AD) is the only facility which provides such a beam available. Figure 1 shows a schematic of the AD ring. At CERN, proton beams accelerated to 26 GeV/c collide with an Ir target to produce antiprotons via the reaction $p + p \rightarrow p + p + p + \bar{p}$. A fraction of them, 5×10^7 in number, are collected by a strong

magnetic horn at 3.6 GeV/c and stored in the AD ring, which are then cooled via electron cooling [13] and stochastic cooling [14] techniques and decelerated down to a momentum of 100 MeV/c or 5.3 MeV in kinetic energy. They are then extracted to experimental zones as a good-quality* pulsed beam consisting of typically 3×10^7 antiprotons in a bunch of 100–200 ns.

Thus produced antiproton beam, though already lower in energy by 3 orders of magnitude than at production, needs further deceleration for them to be captured in vacuo electrostatically. A conventional method using thick degrader foils inevitably caused considerable broadening of the energy spread, and most of the antiprotons either stopped inside the foil or were not decelerated enough to be confined in the prepared potential. At best the capture efficiency was 0.01%–0.1% [15, 16].

In order to decelerate antiprotons efficiently, the ASACUSA collaboration [7] developed a Radio Frequency Quadrupole Decelerator (RFQD) [17] in collaboration with the CERN PS group. RF wave was applied to the cavities in a similar way as in a normal RFQ LINAC, but with opposite phase, to decelerate (instead of accelerating) microbunches of the antiproton beam at 5.3 MeV down to 63 keV, with an efficiency of 30%. Since the RF cavities can be biased ± 60 keV, the output antiproton energy can be varied 10–120 keV.

INJECTION

The output beam from the RFQD was injected into an electromagnetic trap in the strong magnetic field of 2.5 T produced by a superconducting solenoid, via an Low-Energy Beam Transport line (LEBT), as shown in Fig. 2(a).

The beam was focused by a set of pulsed solenoids at LEBT and by the converging magnetic field of the superconducting solenoid to a diameter of 3–4 mm (see Fig. 2(b)). It was injected into the trap through a thin Mylar i.e. PET (polyethylene terephthalate) double-layered foil of $90 \mu\text{g}/\text{cm}^2$ for each layer, used to isolate ultrahigh vacuum (UHV) of 10^{-10} Pa inside the trap from a relatively poor vacuum of 10^{-6} – 10^{-7} Pa in the LEBT. This foil also served as a highly sensitive beam profile monitor for the antiproton beam. Silver was evaporatively plated onto the layers of the foil in a form of ten strips of 1 mm width and 25 nm thickness. Signals from each strips used as electrodes to detect emission of secondary electrons were amplified and read out, which allowed monitoring position and distribution of the penetrating antiproton beam for x and y direction for each layer (thus two-dimensional monitor). An example of the beam profile observed by this monitor is given in Fig. 2(c). For diagnosis of the beam transport at LEBT, we used yet another set of newly developed beam profile monitors consisting of thin wires of 10–20 μm diameter placed with a gap of 1 mm next to each other [18]. These beam profile monitors allowed for the first time non-destructive measurement of the antiproton beam at low energies, which was not possible with MWPCs (Multi-Wire Proportional Chambers), and they proved to be powerful tools in the delicate beam tuning at LEBT.

Taking into account the energy loss in the foil, we varied the bias voltage of the RFQD

* The emittance of the beam is 1π mm mrad and the momental bite is $\Delta p/p \sim 0.1\%$.

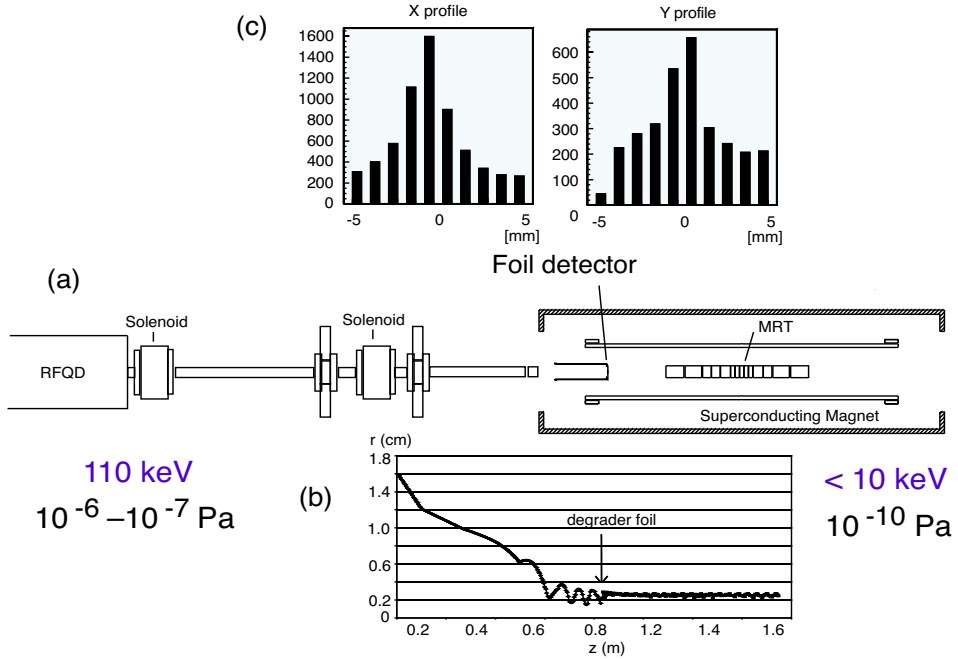


FIGURE 2. (a) Schematic of the LEBT line and the magnet. The antiproton beam out of the RFQD was focused into the foil in the 2.5 T magnetic field. Calculated beam diameter along the LEBT line (b) and an example of the beam profile monitored by the foil detector (c) are also shown.

so as to adjust the antiproton energy after penetration through the foil. In order for the antiprotons to be captured in a high-voltage potential of 10 kV as will be discussed later, their transverse energy should be less than 10 keV after the foil. We placed two Čerenkov detectors, one upstream and one downstream of the superconducting solenoid, in order to know the rough position of antiproton annihilation by detecting annihilation products such as fast charged pions. Figure 3 shows signals from the Čerenkov detectors, read out by a digital oscilloscope. When the antiproton beam was stopped at a closed gate valve #1 (see Fig. 3(a)), two peaks were observed, corresponding to the undecelerated fraction of the beam at 5.3 MeV and the decelerated fraction at 91.5 keV at later time. When the gate valve was opened (b), the second peak moved slightly to a later time, with the time difference due to time of flight, corresponding to annihilation at the position of the degrader foil, placed 40 cm downstream of the gate valve. This means that the antiproton beam has lost the energy and stopped inside the foil. This fact can be confirmed by the signal from the downstream Čerenkov detector (c), showing no peak of decelerated antiprotons reaching downstream. On the other hand, when the incident energy of the antiproton beam out of the RFQD was increased to 121.5 keV (d), little annihilation was observed in the foil, while a large broad peak was observed downstream (e), indicating that most of the antiprotons at 121.5 keV have penetrated through the foil.

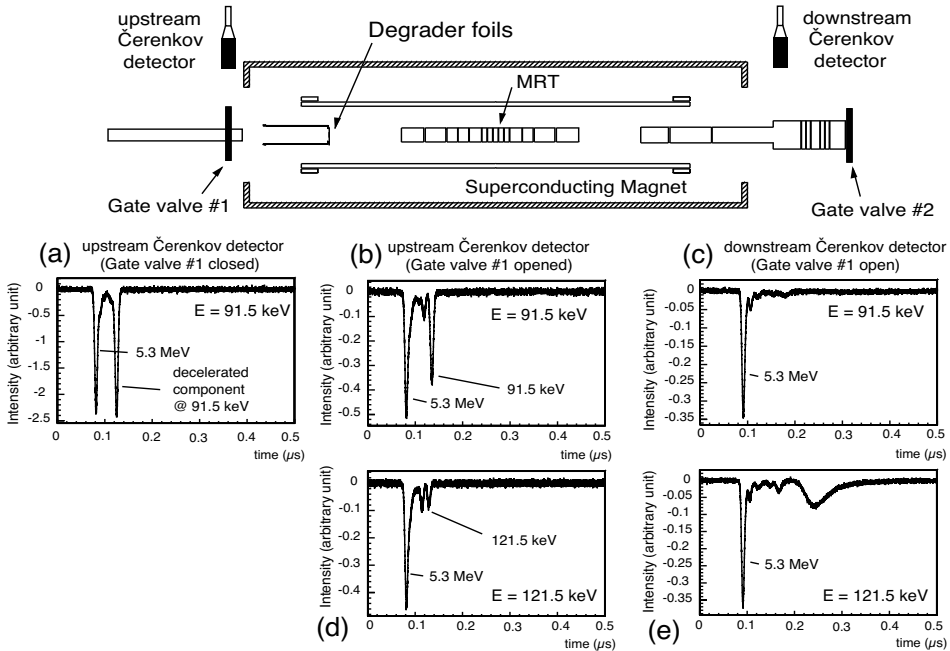


FIGURE 3. Signals from Čerenkov detectors at different conditions, shown together with a schematic of the apparatus. For details see the text.

We then applied a high voltage of 10 keV to the most downstream electrode (among the set of trap electrodes placed in the center of the superconducting magnet) to reflect back the antiproton beam. As shown in Fig. 4 for the case of 111.5 keV injection, the broad peak (A) observed at downstream became smaller (B) after application of the high voltage, because a major fraction of antiprotons bounced back to upstream. The broad peak still remaining corresponds to antiprotons with their energy greater than 10 keV after passage through the foil. By varying the voltage applied, we can measure transverse energy distribution after the foil, as the derivative of the reflection ratio as a function of the potential applied, as shown in Fig. 5. For each voltage, the area of the broad peak was compared between the cases with and without the high voltage, and their ratio was calculated. For example, at the voltage of 10 keV, from Fig. 4 we learn that among the antiprotons which have penetrated through the foil (A), 70% of them were reflected back by the potential toward upstream and disappeared from the downstream Čerenkov signal, while the rest 30% still travelled toward downstream (B). This means that, after the foil, 70% of the antiprotons had a transverse energy of 10 keV or less, and

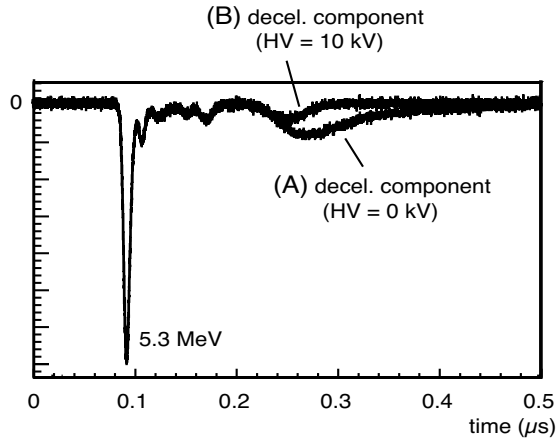


FIGURE 4. Signal from the downstream Čerenkov detector. When no high voltage was applied, the broad peak (A) corresponds to antiprotons with their broad energy variation around 10 keV, after energy degradation in the foil. When a high voltage of 10 kV was applied, the remaining broad peak (B) corresponds to antiprotons with their energy more than 10 keV which reached downstream, while the rest of the antiprotons were reflected by the high voltage and hence were not observed by the downstream Čerenkov detector.

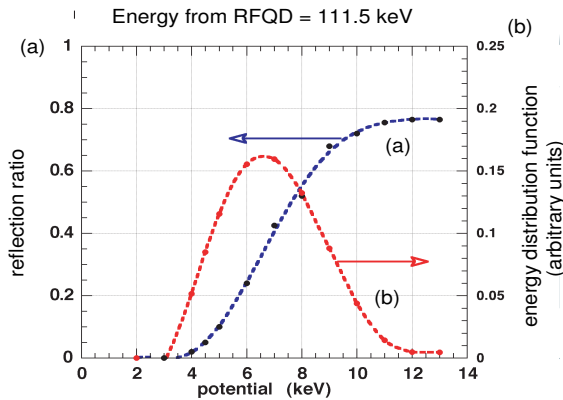


FIGURE 5. Reflection ratio (a) of the antiprotons by high voltage potential and deduced transverse energy distribution (b) of antiprotons after passage through the degrader foil, incident at 111.5 keV.

this number is plotted as graph (a) in Fig. 5. † By differentiating thus obtained curve, the

† The percentage discussed is normalized to the number of antiprotons which have penetrated through the foil. We must note that 30% of incident antiprotons stopped inside the foil under this condition.

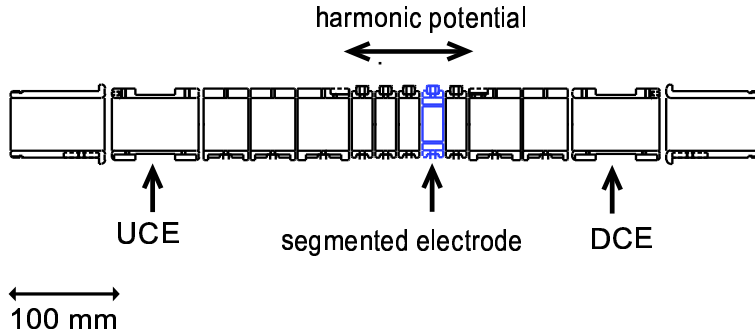


FIGURE 6. A schematic cross section of the MRT along the trap axis.

energy distribution after the foil can be obtained and is plotted as the graph (b). **

CONFINEMENT AND COOLING

Antiprotons were then captured and confined in an electromagnetic trap. We used a Multi-Ring Trap (MRT) [19] consisting of 14 cylindrical electrodes placed coaxially along the magnetic field line, as shown in Fig. 6. A favorable feature of the MRT compared with a normal Penning trap is that a harmonic electric potential can be prepared in a wider region near the trap axis by application of appropriate voltage on each electrode, which allows trapping of a much larger number of charged particles. A large trap volume can be prepared also by a trap with a well-type potential, but the MRT has a superior ability to trap particles far more stably.

Figure 7 shows sequential steps for antiproton capture, cooling and extraction. The pulse of incident antiprotons were reflected backward at the DCE (Downstream Catching Electrode) floated at -10 kV. By the time the pulse returned after its round trip of typically 500 ns back to the UCE (Upstream Catching Electrode), the trap was closed by a fast switch with a rise time of 200 ns which biased the UCE to -10 kV, confining the major part of the antiprotons. The antiprotons were then cooled by a plasma of typically 3×10^8 electrons preloaded in the harmonic potential. Antiprotons lost their energy by transferring it to electrons, while the heated electrons cooled by themselves by emission of synchrotron radiation in the magnetic field of 2.5 T with its time constant of about 1 s, until the antiprotons were trapped in the bottom of the harmonic potential of 50 V depth. We then opened one side of the potential for 550 ns to selectively release electrons: lighter and thus faster electrons escaped within this short period, while heavier and much slower antiprotons remained inside. This release of electron turned out to be

** We assumed here that the position distribution of antiprotons reaching downstream does not depend on the energy, so that the solid angle of the downstream Čerenkov detector for antiproton annihilation is constant.

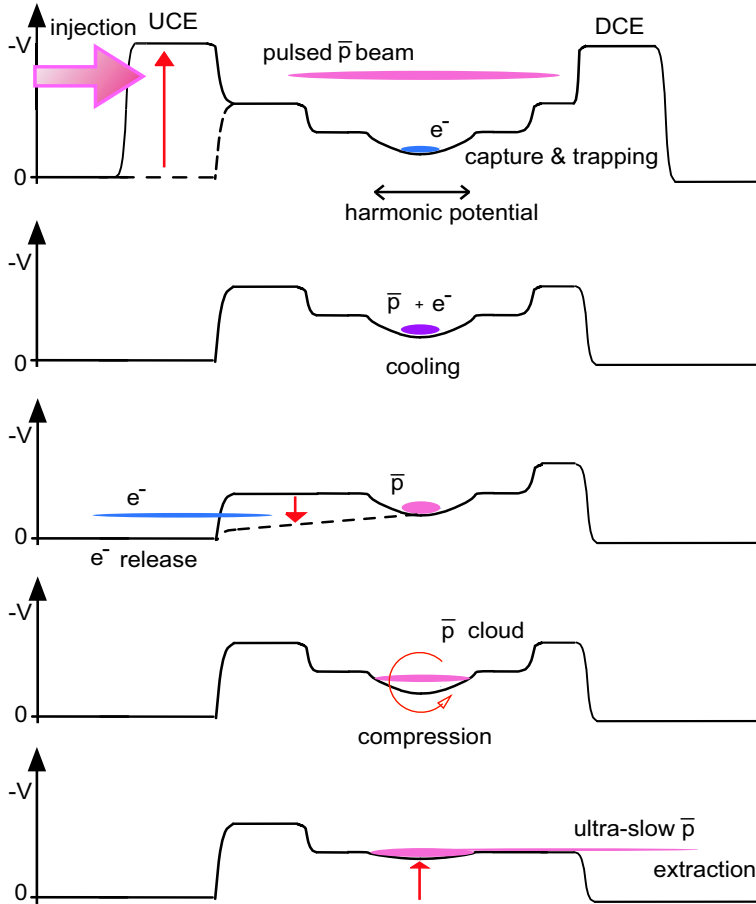


FIGURE 7. Sequential procedures of antiproton capture, cooling and extraction.

essential because our trial of antiproton extraction together with electrons never worked out [20].

The antiproton cloud were then given torque by a rotating electric field to be compressed radially. For this purpose, one of the electrodes was segmented azimuthally into four parts as can be seen in Fig. 6, and an RF voltage was applied to each segment with a phase difference of $\pi/2$ next to each other [21, 22].

As a diagnostic device of antiproton trapping, we prepared a set of track detectors to know the position and time of antiproton annihilation. Two scintillator bars of 2 m in length, with a rectangular cross section of $4(\text{H}) \times 6(\text{V}) \text{ cm}^2$, were placed in the same plane and parallel to the trap axis, as shown in Fig. 8(a). Passage of charged particles such as pions, or electron-positron showers converted from gamma rays originating in

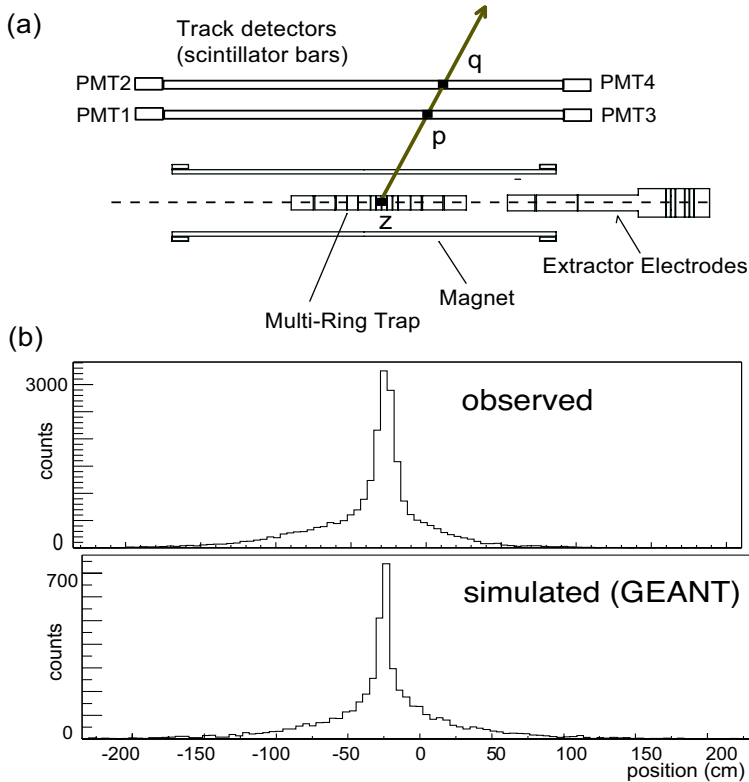


FIGURE 8. (a) Position of antiproton annihilation can be calculated from the trajectory of produced particles, detected by scintillator bars. (b) Observed position resolution agreed with our simulation using GEANT code.

the decay of neutral pions, was detected and the position of the hit points (shown as ‘p’ and ‘q’ in the figure) was calculated from the time-of-flight difference of the scintillation light, arriving at photomultiplier tubes (PMT) at both ends of the bars. Tracking back the reconstructed particle trajectory back onto the trap axis, antiproton annihilation (‘z’ in the figure) can be detected with a position resolution of 20 cm and with a detection efficiency of typically $\varepsilon = 5\%$, which agreed with our simulation [23] using GEANT trajectory calculation code [24] (see Fig. 8(b))[‡].

Figure 9 shows detected annihilation counts as a function of time and position along the beam axis (i.e. the trap axis). Frequent annihilation was observed at early times

[‡] The detection efficiency is primarily determined by the solid angle of the detector and the multiplicity of pions. Relatively bad position resolution is due to scattering of electron-positron showers in the thick material of the magnet. The showers originate in gamma rays from the decay of neutral pions.

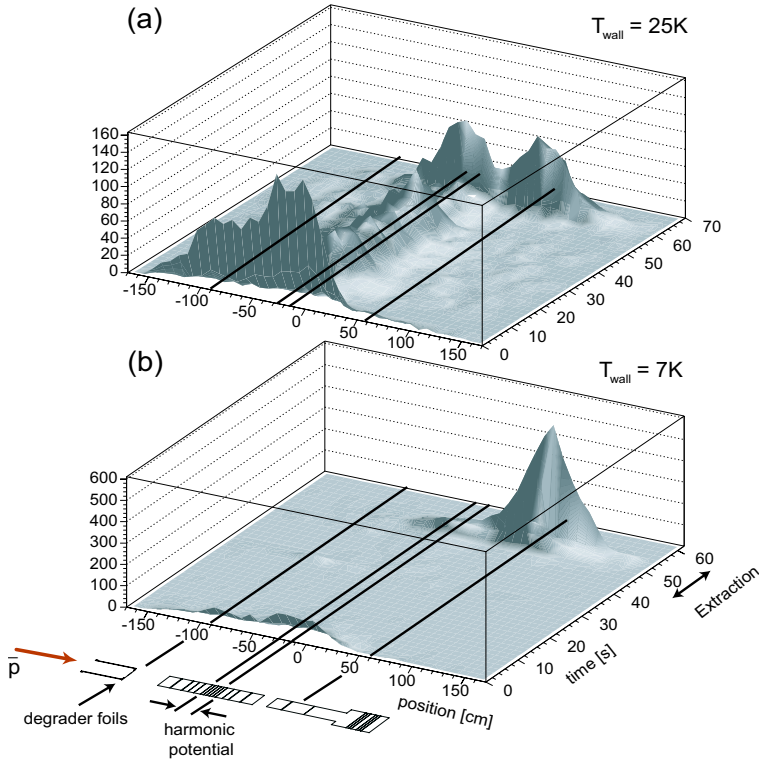


FIGURE 9. Annihilation counts observed as a function of time and position.

for a typical period of 10 s following antiproton injection at $t = 0$. They occurred at positions of the degrader foil and the trap. After the antiprotons have been cooled enough, there still remained constant annihilation in the trap center when the temperature of the bore which housed the trap electrodes was 25 K (top figure (a)). This was due to continuous antiproton annihilation against atomic nuclei of residual gases, mainly hydrogen. A standard “ultra-high” vacuum is not apparently good enough for stable confinement of antiprotons. On the other hand, no annihilation was observed during confinement at the bore temperature of 7 K (bottom figure (b)). At this cryogenic temperature, even the hydrogen gas froze out and an extremely high vacuum better than 10^{-10} Pa was achieved, preventing antiproton annihilation. Since the vacuum is very sensitive to the ambient temperature, stable cryogenic cooling was important in stable antiproton trapping. Antiprotons were then extracted and many annihilations were observed downstream of MRT.

Integrating the number of antiproton annihilations over all the positions, we obtain total number of antiprotons. Figure 10 shows cumulative count of antiproton annihilation as a function of time. The rapid increase at the last stage of the trapping cycle

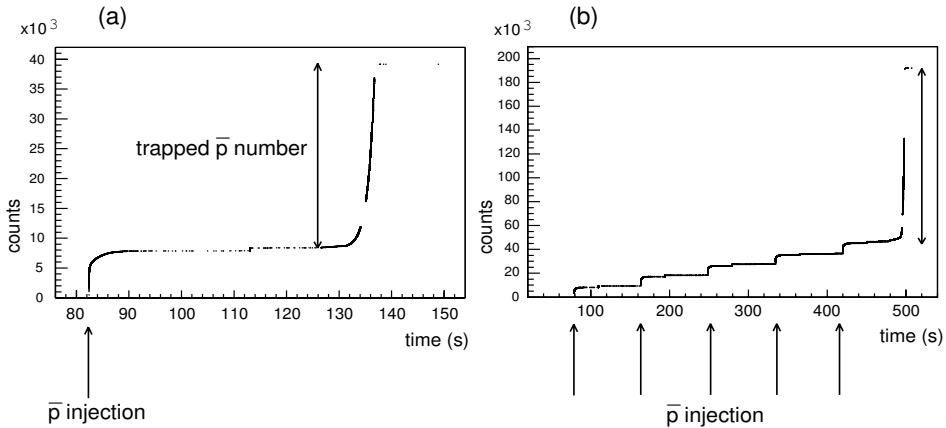


FIGURE 10. Cumulative number of antiproton annihilation as a function of elapsed time. The total number of antiprotons in the trap was (a) 1.2 million for a single AD shot and (b) 4.8 million for stacking of 5 AD shots.

corresponds to the antiprotons which were confined stably. Taking into account the detection efficiency ε of antiproton annihilation by the track detectors, we concluded that 1.2×10^6 antiprotons were trapped stably until the end of our trap cycle of 1–5 minutes [20]. Typically 1 million antiprotons were trapped for each AD shot. We then accumulated antiprotons for several AD shots (see Fig. 10(b)). This technique of “stacking” also worked fine, and we trapped 4.8×10^6 antiprotons simultaneously for stacking of 5 AD shots, the largest number of antiprotons ever accumulated.

EXTRACTION AND BEAM TRANSPORT

The antiprotons were then released from the trapping potential as it was gradually shallowed, and were extracted as an ultra-slow continuous beam of 10–500 eV. Since the antiprotons tend to expand in radial direction when they follow the strongly diverging magnetic field line out of the 2.5 T magnetic field, it was essential that the antiproton cloud be well compressed radially in the trap. This was achieved by application of rotating electric field [22]. Also important in efficient extraction was precise alignment. The magnetic field axis, electric trap axis, the beam transport axes: all these needed to be well aligned precisely.

The extraction beamline was designed to transport antiproton beams over a length of 3 m, at variable energies ranging from 10 to 1000 eV. The antiproton beams were refocused three times by sets of Einzel lenses at the position of apertures, as shown in Fig. 11. These variable apertures of diameter 4–10 mm allow differential pumping of 6 orders of magnitude along the beamline, which was necessary to keep the trap region at an extremely high vacuum better than 10^{-10} Pa so as to avoid antiproton annihilation, while the end of the beamline will be exposed to atomic or molecular gas jets of upto

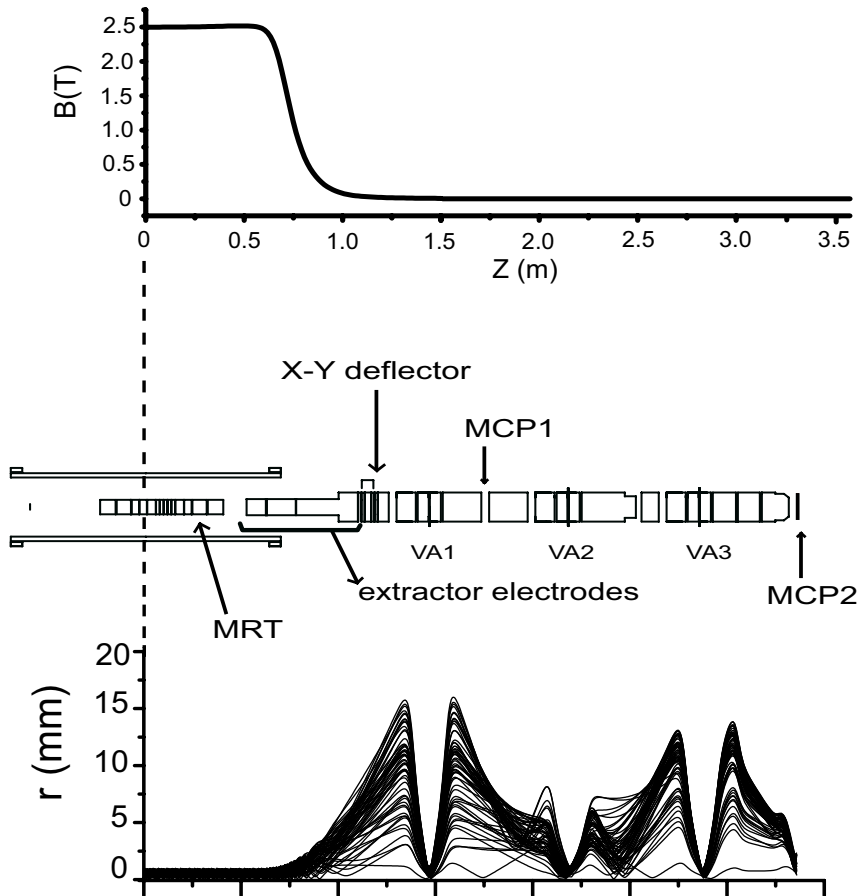


FIGURE 11. Schematic of the extraction beamline for ultra-slow antiproton beams. The beams are focused 3 times at positions of variable apertures, to comply with the requirement of effective differential pumping (bottom). Magnetic field strength is also shown in the top figure.

10^{-4} Pa [25]

The MRT, the superconducting solenoid and the eV-beam transport line are jointly known as “MUSASHI”, or the Monoenergetic Ultra-Slow Antiproton Source for High-precision Investigations. MUSASHI opens a new research field ranging from atomic physics to nuclear physics [10], including our near-future project of antihydrogen synthesis in a cusp trap [12]. As from nuclear physics point of view, low-energy antiproton is suited to give information on nuclear peripherals [10, 26, 27, 28], but it would be more interesting from atomic-physics point of view.

Especially, atomic formation and ionization processes by low-energy antiprotons can be studied under single collision conditions for the first time, and theoretical calcula-

tions [29] will now be tested experimentally. Taking advantage of the slow extraction i.e. continuous aspect of the beam, event-by-event data acquisition becomes possible, associated with each single antiproton. We are now preparing a supersonic gas-jet target for atomic collision experiments planned in the next years. The target is aimed to achieve a density of $3 \times 10^{13} \text{ cm}^{-3}$ with a gas-jet cross section of $5 \text{ mm} \times 1 \text{ cm}$, which will be crossed with the ultra-slow antiproton beams to produce antiprotonic atoms [30].

SUMMARY

With the combination of a RFQD and a MRT in the superconducting solenoid, we have successfully decelerated antiprotons from 5 MeV to less than 10 keV, confined them and cooled them down to sub-eV energies with preloaded electrons. Out of 30 million antiprotons delivered from the AD, 1.2 million antiprotons were trapped stably for a cycle of a few minutes, which was 50 times more efficient than the conventional method of using thick degrader foils for deceleration. Antiprotons were extracted at energies of 10–500 eV, and this continuous ultra-slow antiproton beam will be a powerful tool for the study of atomic collision dynamics and formation of antiprotonic atoms including antihydrogen, as well as nuclear physics.

ACKNOWLEDGMENTS

We are grateful to the AD and PS staff in the AB department of CERN for their tireless effort in providing us with the antiproton beam. We acknowledge Mr. W. Pirkl and his team for their engagement in the design and operation of the RFQD. This work was supported by the Grant-in-Aid for Creative Scientific Research (10P0101) of the Japanese Ministry of Education, Culture, Sports, Science and Technology (MonbuKagaku-shō), Special Research Projects for Basic Science of RIKEN, and the Hungarian National Science Foundation (OTKA T033079).

REFERENCES

1. O. Chamberlain, E. Segrè, C. Wiegand, and T. Ypsilantis, *Phys. Rev.* **100**, 947 (1955).
2. CPLEAR Collaboration, A. Angelopoulos *et al.*, *Phys. Lett. B* **420**, 191 (1998).
3. G. Baur *et al.*, *Phys. Lett. B* **368**, 251 (1996).
4. CERN Antiproton Decelerator web page, <http://psdoc.web.cern.ch/PSdoc/acc/ad/index.html>
5. M. Amoretti *et al.*, *Nature* **419**, 456 (2002).
6. G. Gabrielse *et al.*, *Phys. Rev. Lett.* **89**, 213401 (2002).
7. ASACUSA collaboration web page, <http://cern.ch/ASACUSA>
8. M. Hori, J. Eades, R.S. Hayano, T. Ishikawa, W. Pirkl, E. Widmann, H. Yamaguchi, H.A. Torii, B. Juhász, D. Horváth, and T. Yamazaki, *Phys. Rev. Lett.* **91**, 123401 (2003).
9. S.P. Møller, A. Csete, T. Ichioka, H. Knudsen, U.I. Uggerhøj, and H.H. Andersen, *Phys. Rev. Lett.* **88**, 193201 (2002).
10. Y. Yamazaki, *Nucl. Instrum. Methods in Phys. Res. B* **154**, 174 (1999).
11. ASACUSA collaboration, proposal submitted to CERN/SPSC, CERN/SPSC 97-19; CERN/SPSC 2000-04; CERN-SPSC 2005-002.

12. A. Mohri and Y. Yamazaki, *Europhys. Lett.* **63**, 207 (2003); A. Mohri, “Non-Neutral Plasma Confinement in a Cusp-Trap and Possible Application to Anti-Hydrogen Beam Generation”, Contribution to Workshop on Physics with Ultra Slow Antiproton Beams, RIKEN, March 2005 (in this book).
13. G.I. Budker, *Proc. Int. Symp. On Electron and positron storage rings, Saclay*, ed. by H. Zyngier and E. Cremieux-Alcan (PUF, Paris, 1967) p.II-1-1; S.P. Vytchanin, *Sov. Phys. Dokl.* **22**, 321 (1977); G.I. Budker and A.N. Skrinski, *Sov. Phys. Usp.* **21**, 277 (1978).
14. S. van der Meer, Stochastic Cooling and the Accumulation of Antiprotons, *Nobel lecture (1984)*; Stochastic cooling in the Antiproton Accumulator, *IEEE Trans. Nucl. Sci.* **NS28**, 1994 (1981).
15. G. Gabrielse *et al.*, *Phys. Lett. B* **548**, 140 (2002).
16. M. Amoretti *et al.*, *Nucl. Instrum. Methods in Phys. Res. A* **518**, 679 (2004).
17. A. M. Lombardi, W. Pirkel, and Y. Bylinsky, in *Proceedings of the 2001 Particle Accelerator Conference, Chicago, 2001* (IEEE, Piscataway, NJ, 2001), pp. 585–587.
18. M. Hori, *Nucl. Instrum. Methods. A* **522**, 420 (2004).
19. A. Mohri, H. Higaki, H. Tanaka, Y. Yamazawa, M. Aoyagi, T. Yuyama, and T. Michishita: *Jpn. J. Appl. Phys.* **37**, 664 (1998).
20. N. Kuroda, H. A. Torii, K. Yoshiki Franzen, Z. Wang, S. Yoneda, M. Inoue, M. Hori, B. Juhász, D. Horváth, H. Higaki, A. Mohri, J. Eades, K. Komaki, and Y. Yamazaki, *Phys. Rev. Lett.* **94**, 023401 (2005).
21. H. Higaki, N. Kuroda, K. Yoshiki Franzen, Z. Wang, M. Hori, A. Mohri, K. Komaki, and Y. Yamazaki, *Phys. Rev. E* **70**, 026501 (2004).
22. N. Kuroda *et al.*, “Control of plasmas for production of ultraslow antiproton beams”, Contribution to Workshop on Physics with Ultra Slow Antiproton Beams, RIKEN, March 2005 (in this book).
23. S. Yoneda, master thesis, Department of Physics, University of Tokyo, in *Japanese* (2003); D. Barna, private communication (2004).
24. GEANT3, CERN Program Library Long Writeup W5013.
25. K. Yoshiki Franzen, N. Kuroda, H.A. Torii, M. Hori, Z. Wang, H. Higaki, S. Yoneda, B. Juhász, D. Horváth, A. Mohri, K. Komaki, and Y. Yamazaki, *Rev. Sci. Instrum.* **74**, 3305 (2003).
26. A. Trzcińska *et al.* Neutron Density Distributions Deduced from Antiprotonic Atoms, *Phys. Rev. Lett.* **87**, 82501 (2001).
27. J. Jastrzebski *et al.* *Nucl. Phys. A* **588**, 405c (1993).
28. M. Wada and Y. Yamazaki, *Nucl. Instr. Meth. B* **214**, 196 (2004).
29. J. S. Cohen, *Rep. Prog. Phys.* **67**, 1769–1819 (2004).
30. V. L. Varentsov *et al.*, “ASACUSA Gas-Jet Target: Present Status And Future Development”, Contribution to Workshop on Physics with Ultra Slow Antiproton Beams, RIKEN, March 2005 (in this book).